Biogeosciences Discuss., 5, 4235–4270, 2008
www.biogeosciences-discuss.net/5/4235/2008/

Biogeosciences Discussions is the access reviewed discussion forum of *Biogeosciences*

Satellite-detected fluorescence reveals global physiology of ocean phytoplankton

M. J. Behrenfeld[1], T. K. Westberry[1], E. S. Boss[2], R. T. O'Malley[1], D. A. Siegel[3], J. D. Wiggert[4], B. A. Franz[5], C. R. McClain[5], G. C. Feldman[5], S. C. Doney[6], J. K. Moore[7], G. Dall'Olmo[1], A. J. Milligan[1], I. Lima[6], and N. Mahowald[8]

[1]Department of Botany and Plant Pathology, Cordley Hall 2082, Oregon State University, Corvallis, OR 97331-2902, USA
[2]School of Marine Sciences, 5706 Aubert Hall, University of Maine, Orono, Maine 04469-5741, USA
[3]Institute for Computational Earth System Science and Department of Geography, University of California, Santa Barbara, Santa Barbara, CA 93106-3060, USA
[4]Department of Marine Sciences, University of Southern Mississippi, 1020 Balch Blvd., Stennis Space Center, MS 39529-9904, USA
[5]NASA Goddard Space Flight Center, Greenbelt, MD 20771, USA
[6]Department of Marine Chemistry and Geochemistry, Woods Hole Oceanographic Institution Woods Hole, MA 02543-1543, USA

[7]Department of Earth System Science, 3214 Croul Hall, University of California, Irvine, CA 92697-3100, USA
[8]Cornell University, 2140 Snee Hall, Ithaca, NY 14850 15, USA

Received: 28 August 2008 – Accepted: 3 September 2008 – Published: 5 November 2008

Correspondence to: M. Behrenfeld (behrenfm@science.oregonstate.edu)

Abstract

Phytoplankton photosynthesis links global ocean biology and climate-driven fluctuations in the physical environment. These interactions are largely expressed through changes in phytoplankton physiology, but physiological status has proven extremely challenging to characterize globally. Phytoplankton fluorescence does provide a rich source of physiological information long exploited in laboratory and field studies, and is now observed from space. Here we use satellite-based fluorescence measurements to evaluate light-absorption and energy-dissipation processes influencing phytoplankton light use efficiency and demonstrate its utility as a global physiological indicator of iron-limited growth conditions. This new tool provides a path for monitoring climate-phytoplankton physiology interactions, improving descriptions of light use efficiency in ocean productivity models, evaluating nutrient-stress predictions in ocean ecosystem models, and appraising phytoplankton responses to natural iron enrichments or purposeful iron fertilizations activities.

1 Introduction

Phytoplankton are taxonomically-diverse, single-celled organisms that populate the upper sunlit layer of nearly all water bodies on Earth, and they are photosynthetic. Net annual photosynthesis by ocean phytoplankton alone is of similar magnitude as that by all terrestrial plants (Field et al., 1998; Behrenfeld et al., 2001) and it plays a vital role in biospheric carbon cycling. Ocean productivity is strongly impacted by climate variations (Behrenfeld et al., 2006a), but quantifying this impact and predicting future change requires an understanding of environmental factors regulating phytoplankton light use efficiencies and growth (Behrenfeld et al., 2008). However, globally characterizing physiological variability has proven far more challenging than simply quantifying phytoplankton standing stocks. In 2002, the Moderate-resolution Imaging Spectroradiometer (MODIS) sensor was launched on NASA's Aqua satellite platform with a

capacity to detect phytoplankton chlorophyll fluorescence, in hope that these measurements would yield new insights into phytoplankton physiological status.

As with terrestrial plants, oxygenic photosynthesis in phytoplankton involves light harvesting and electron transport between two pigmented reaction centers: photosystem II (PSII), which is solely responsible for oxygen evolution, and photosystem I (PSI), where light energy is captured in chemical form. Both photosystems contribute to cellular chlorophyll concentration and light absorption, but in vivo fluorescence emanates almost exclusively from pigments at the core of PSII alone (Falkowski and Kiefer, 1985). Accordingly, detailed measurements of stimulated fluorescence induction have been widely used to study PSII functioning, demonstrating that fluorescence yields are strongly influenced by light and nutrient growth conditions (Krause and Weis, 1991; Falkowski and Kolber, 1995; Behrenfeld et al., 2006b). Fluorescence emission under natural sunlight can also be detected in subsurface- and above-surface upwelling irradiance spectra (Neville and Gower, 1977; Morel and Prieur, 1977). This "natural fluorescence" signal was proposed originally as a tool for deriving phytoplankton photosynthetic rates (Topliss and Platt, 1986; Kiefer et al., 1989) and has been demonstrated to register physiological variability (Letelier et al., 1997; Morrison 2003). Such field observations were instrumental to the development of satellite fluorescence detection capabilities.

To date, application of satellite chlorophyll fluorescence observations has been limited and largely focused on geographically-restricted studies assessing near-shore chlorophyll concentrations or detecting harmful algal species (e.g., Gower et al., 2004; Hu et al., 2005; Ahn and Shanmugam, 2007; Gilerson et al., 2007, 2008; Gower and King, 2007; Huot et al., 2007). Here, satellite-based chlorophyll fluorescence data are presented at the full global scale and evaluated as a physiological indicator. We find that three primary factors regulate global fluorescence distributions: (1) phytoplankton pigment concentrations, (2) a photoprotective response aimed at preventing high-light damage (i.e., "non-photochemical quenching"), and (3) "pigment packaging", a self-shading phenomenon influencing light absorption efficiencies (Duysens, 1956;

Bricaud et al., 1995, 1998). Additional information on nutrient stressors is resolved by first accounting for these three primary factors and then deriving global distributions of fluorescence quantum yield, the ratio of photons fluoresced per photons absorbed. As described below, iron-stress was anticipated a priori to be a key factor influencing satellite quantum yields (Behrenfeld et al., 2006b, 2008), and this expectation is upheld by a close correspondence between elevated satellite fluorescence yields and low-iron conditions predicted from ecosystem models with active iron cycling. Our results present satellite fluorescence quantum yields as an important new tool for characterizing iron stress in the global oceans, provide a path for improving ocean photosynthesis estimates and resolving climate-phytoplankton interactions, and identify key directions for future research to further mine the rich physiological information imprinted on satellite chlorophyll fluorescence fields.

2 Data and analyses

2.1 Fluorescence from space

Chlorophyll fluorescence (F) is only a minor de-excitation pathway for sunlight energy absorbed by phytoplankton, but it creates a distinct shoulder in the color spectrum of the ocean (Neville and Gower, 1977). In the field, this flux of radiance is readily resolved and frequently modeled as the product of chlorophyll concentration (Chl), the spectrally-averaged, chlorophyll-specific phytoplankton absorption coefficient ($< a^*_{ph} >$), the flux of photosynthetically active radiation ($iPAR$), and the quantum yield of fluorescence (ϕ) (e.g., Kiefer et al., 1989):

$$F = \mathrm{Chl} \times < a^*_{ph} > \times iPAR \times \phi. \quad (1)$$

Equation (1) highlights fundamental dependencies of solar-induced fluorescence emission, but additional factors must be considered when extracting the phytoplankton fluorescence signal from space (Huot et al., 2005). Here, an overview is given on our

treatment of MODIS satellite fluorescence data, while a detailed step-wise description is provided in Appendix A.

Global open-ocean phytoplankton chlorophyll fluorescence (F_{sat}) distributions were investigated using standard monthly MODIS-Aqua fluorescence line height products generated by NASA's ocean color processing group (http://oceancolor.gsfc.nasa.gov) for the period January 2003 to December 2007. Radiances measured by the 10 nm-wide fluorescence band on MODIS include both atmospheric and oceanic components, cover only a portion of the chlorophyll fluorescence emission spectrum, and are centered at 678 nm rather than the emission peak at 685 nm (to avoid an atmospheric oxygen absorption feature). The atmospheric component is removed during standard processing using measurement bands in the near-infrared. The residual oceanic component of the fluorescence band signal includes contributions from chlorophyll fluorescence, backscattered sunlight, and Raman scattered sunlight. The two latter components (backscatter and Raman) are accounted for by calculating a 678 nm "baseline radiance" through linear extrapolation of radiances measured at 667 and 748 nm (Abbott and Letelier 1999, Huot et al., 2005). Subtraction of this "baseline" from the 678 nm signal yields the fluorescence line height product (Appendix A).

As detailed in Appendix A, conversion of fluorescence line height data into F_{sat} requires additional adjustments accounting for satellite viewing geometry, attenuation in the water column of downwelling solar radiation and upwelled fluoresced light, differences between the MODIS fluorescence detection band and the chlorophyll emission spectrum, the fraction of isotropically emitted fluorescence propagating in the upward direction, and the top-of-atmosphere irradiance.

Combining these corrections into a single term (S), a simplified expression emerges relating global satellite fluorescence (F_{sat}) to four primary variables:

$$F_{sat} = Chl_{sat} \times <a^*_{ph}> \times \phi \times S, \quad (2)$$

where Chl_{sat} is satellite-derived surface-layer chlorophyll concentration and S is approximately 100 mW cm^{-2} μm^{-1} sr^{-1} m (Appendix A).

While our treatment of MODIS fluorescence data is similar in many respects to earlier studies (e.g., Abbott and Letelier, 1999; Huot et al., 2005), a few important differences exist. First, a critical distinction is made between Eq. (1) and (2) in that the latter does not include *iPAR*. This difference results because fluorescence line height data used for calculating F_{sat} are derived from radiances normalized to the downwelling light at the sea surface i.e., "normalized water leaving radiance": $L_{WN}(\lambda)$. Consequently, the direct dependence of F_{sat} on *iPAR* is already removed (Appendix A). This property of line height products has been overlooked in earlier treatments, resulting in additional division by *iPAR* in quantum yield calculations and introduction of errors into derived fields. A second difference in our analysis is the treatment of negative fluorescence values. In earlier studies, these negative values were eliminated by adding an arbitrary fluorescence constant. This "constant" impacted ϕ estimates in low chlorophyll waters, initially having a value equal to the fluorescence of 1 mg Chl m^{-3} (Abbott and Letelier, 1999) and later revised downward (Huot et al., 2005). We do not add an arbitrary constant. Instead, we removed the affected pixels because they represented only 0.2% of the MODIS data, are randomly distributed globally, and likely represent pixels with unflagged atmospheric correction problems. Finally, we impose the first-principles constraint that F_{sat}=0 when Chl_{sat}=0 (i.e., there can be no chlorophyll fluorescence when there is no chlorophyll). Regression analysis of F_{sat} on Chl_{sat} indicates that this constraint is satisfied by subtracting a small value of 0.001 mW cm^{-2} μm^{-1} sr^{-1} from F_{sat}, which is well within the radiometric uncertainty of ±0.003 mW cm^{-2} μm^{-1} sr^{-1} for the MODIS fluorescence band (see http://oceancolor.gsfc.nasa.gov/VALIDATION/operational_gains.html).

2.2 Aeolian soluble iron deposition

To investigate relationships with nutrient stressors, fluorescence quantum yields calculated from F_{sat} data were initially compared to surface nitrate and phosphate climatologies from the World Ocean Atlas (Garcia et al., 2006) and global distributions of

modeled aeolian soluble iron deposition. Deposition of soluble iron was estimated using a three-dimensional model of dust entrainment, transport, deposition, and solubility (Luo et al., 2003, 2008; Mahowald et al., 2003). The model is driven by reanalysis winds from the National Center for Environmental Prediction/National Center for Atmospheric Research (Kistler et al., 2001) that represent a combination of observations and model output for a given time period. Entrainment of dust into the atmosphere is simulated using the Dust Entrainment and Deposition module (Zender et al., 2003), while removal is through wet and dry deposition processes. Compared to observations, the model does well in simulating dust cycles in most regions, but may yield an overestimate of dust deposition in some remote Southern Hemisphere ocean regions based on comparisons with the few measurements available (Luo et al., 2003; Wagener et al., 2008). This overestimate of deposition may be partially compensated for, however, by an underestimate of the soluble iron fraction in remote regions (Luo et al., 2005, 2008).

3 Results and discussion

3.1 Factors dominating satellite fluorescence

Spatial patterns in F_{sat} are correlated to first order with Chl_{sat}, as illustrated in Fig. 1 using July 2004 images. Thus, F_{sat} is high wherever surface nutrient levels are sufficient to support significant phytoplankton biomass (i.e., enhanced chlorophyll). Such areas include equatorial and coastal upwelling waters, as well as high latitude regions of the North Atlantic and Southern Ocean where strong seasonal phytoplankton blooms occur (Fig. 1). Conversely, both F_{sat} and Chl_{sat} are persistently low in the nutrient-impoverished, permanently stratified central ocean gyres (Fig. 1). The relationship between F_{sat} and Chl_{sat} is not globally consistent, however, and the extent of these deviations becomes clear when monthly satellite data for our 5 year MODIS record are aggregated into regional bins (Fig. 2a) (Behrenfeld et al., 2005) (*Appendix A, Fig. A1*).

Variability in the F_{sat} versus Chl_{sat} relationship (Fig. 2a) reflects variations in the re-

maining terms of Eq. (2), particularly $<a^*_{ph}>$ and ϕ. A prominent phenomenon influencing phytoplankton absorption coefficients ($<a^*_{ph}>$) is "pigment packaging", which refers to the reduction in $<a^*_{ph}>$ with increasing chlorophyll levels (Duysens, 1956; Bricaud et al., 1995, 1998). Pigment packaging causes a curvilinear relationship between fluorescence and chlorophyll (red line in Fig. 2b) because fluorescence is proportional to light absorption, not simply pigment concentration (Gower et al., 2004; Huot et al., 2005).

Incident light level (*iPAR*) is a prominent factor influencing variability in fluorescence quantum yields (ϕ) through its effect on the saturation state of photosynthesis. Specifically, when a population of phytoplankton acclimated to a given light level is exposed to increasing *iPAR*, light absorption increases linearly with light (blue line in Fig. 3a), while light energy delivered to the core antennae of photosystem II (PSII) saturates. A fraction of the energy arriving at the PSII core is lost as fluorescence (green line in Fig. 3a). Division of this fluorescence emission by total absorbed light energy gives the light-dependance of ϕ (gray line in Fig. 3a – which is the green line divided by the blue line, but note that the two lines are on different relative y-axes, i.e., fluoresced energy is a small fraction of absorbed energy at all light levels). Primary features of the ϕ-*iPAR* relationship are the initial rise in fluorescence as PSII reaction centers become light-saturated and photochemically "closed", followed by a precipitous decrease at higher light levels (Fig. 3a). Commonly, the ϕ-*iPAR* relationship is illustrated using log-transformed *iPAR* data to emphasize variations in ϕ at low light (Morrison, 2003; Schallenberg 2008) (e.g., Fig. 3b). However, it is the rapid decrease in ϕ at supersaturating light that is especially important to F_{sat} analyses because MODIS data are only collected under near-noon, clear-sky conditions when incident sunlight is maximal and supersaturating (*iPAR* during MODIS observations ranges from 500 to 2100 μmole photons m^{-2} s^{-1}, Fig. 2c). At these high light levels, excess absorbed light energy is dissipated as heat by processes collectively termed "nonphotochemical quenching" (NPQ) (Krause and Weis, 1991; Müller et al., 2001). For a phytoplankton population acclimated to a given light level, these NPQ-driven reductions in ϕ at supersaturating light levels are closely approximated as an inverse function of light ($^1/_{iPAR}$)

(red line in Fig. 2c, 3a, b) (this result is apparent in Fig. 3a where fluorescence is constant (green line) over the range of MODIS iPAR values, while absorbed light increases linearly (blue line), causing the ratio of the two to follow an inverse light function).

The influence of pigment packaging on satellite-sensed fluorescence can be illustrated by comparing NPQ-corrected F_{sat} with Chl_{sat} (Fig. 2b). The resultant relationship closely follows field-observed changes in phytoplankton absorption with increasing chlorophyll (red line in Fig. 2b), thereby allowing correction of F_{sat} for pigment packaging using published $< a^*_{ph} >$ values (Bricaud et al., 1998) (Appendix A). The influence of NPQ is likewise illustrated by comparing package-corrected, chlorophyll-specific F_{sat} with *iPAR* (Fig. 2d). In this case, the resultant relationship generally follows the anticipated inverse function of light (red line in Fig. 2d), which provides an initial correction of F_{sat} for NPQ (deviations from this initial NPQ model are discussed below). Applying these two corrections to our F_{sat} data results in a greatly improved relationship between F_{sat} with Chl_{sat} (r=0.96) (Fig. 2e). Moreover, log-transformation of these quantities reveals a uniform distribution of scatter across the full range of open ocean chlorophyll concentrations (Fig. 2f) that is insensitive to choice of Chl_{sat} algorithm (*Appendix A, Fig. A2*).

In the next section, we continue our analysis of F_{sat} variability by considering potential contributions of nutrient stressors. Before proceeding though, it is worth noting that the findings presented in Fig. 2 provide a clear demonstration of the dominant role of chlorophyll variability, pigment packaging, and NPQ on global F_{sat} distributions. While the two later phenomena have been the subject of extensive earlier field and laboratory investigations (e.g., Duysens, 1956; Krause and Weis, 1991; Bricaud et al., 1995, 1998; Müller et al., 2001), satellite fluorescence reveals their expression on a scale simply inaccessible at ground level, inviting reflection on their global implications.

To provide a quantitative illustration of pigment packaging impacts on ocean chlorophyll concentrations, we used monthly MODIS Chl_{sat} data to calculate global distributions of light absorption from published $<a^*_{ph}>$ estimates (Bricaud et al., 1998). We then estimated the chlorophyll concentrations necessary to achieve an equiv-

alent global distribution of light absorption but with a constant value for $<a^*_{ph}>$ of 0.027 m^2 mg chl^{-1} (i.e., the relatively unpackaged, spectrally-averaged value for $<a^*_{ph}>$ at Chl_{sat}=0.03 mg m^{-3}). This calculation indicates that, in the absence of packaging effects, current annual ocean productivity could be achieved with less than half the contemporary global chlorophyll concentration. This simple result emphasizes the substantial nutrient-resources expended by phytoplankton on additional pigment synthesis to offset reductions in absorption efficiency caused by the pigment packaging phenomenon. To illustrate the impact of NPQ, phytoplankton light absorption ($=<a^*_{ph}>\times$Chl$\times iPAR$) was compared to light utilization for photosynthesis (a saturating function of $iPAR$) under clear sky conditions at the equator. For these calculations, we assumed a relatively high-light acclimated phytoplankton population, with photosynthesis saturating at 250 μmole quanta m^{-2} s^{-1}. This scenario results in 20% of absorbed light energy being used for photosynthesis, while the remaining excess 80% of absorbed light energy must be dissipated as heat by NPQ. Repeating this calculation for any lower-light acclimated population results in a smaller fraction of absorbed light energy being used for photosynthesis and a greater fraction dissipated through NPQ. Clearly, pigment packaging and NPQ are significant aspects of the physiological-ecology of phytoplankton in nature, and are directly link to photosynthetic light use efficiencies.

3.2 Nutrient stress and fluorescence yields

Globally characterizing specific nutrient stressors for phytoplankton growth and photosynthesis has proven difficult historically and was a key motivation for developing satellite fluorescence capabilities. This physiological information resides in the residual F_{sat} variability not accounted for by chlorophyll concentration, pigment packaging, and NPQ (i.e., the remaining scatter in Fig. 2e, f), and is revealed in satellite fluorescence quantum yields (ϕ_{sat}):

$$\phi_{sat}=F_{sat}\times(Chl_{sat}\times<a^*_{ph}>\times S)^{-1}\times{}^{iPAR}/_{\overline{iPAR}}=0.00024\times F_{sat}\times iPAR\times Chl_{sat}^{-0.657}, \quad (3)$$

where ${}^{iPAR}/_{\overline{iPAR}}$ represents an inverse-light correction for NPQ that normalizes ϕ_{sat} to the average *iPAR* for MODIS ($\overline{iPAR}$) of 1590 μmole photons $m^{-2}\,s^{-1}$ (Appendix A).

Applying Eq. (3) yields a global average value for ϕ_{sat} of 0.4%, which corresponds well to high-light quantum yields measured in the field (Morrison, 2003). As an initial test of nutrient stress effects, seasonal distributions of ϕ_{sat} (e.g., Fig. 4a) were compared to climatological surface nitrate and phosphate fields (Fig. 4b, c), with no apparent correspondence found between elevated ϕ_{sat} and low macronutrient levels. However, when ϕ_{sat} is compared to the aeolian deposition of soluble iron (a proxy for iron stress) (Luo et al., 2003; Mahowald et al., 2003; Luo et al., 2008), a clear agreement emerges (Fig. 4a, d). Specifically, we find elevated ϕ_{sat} values (>0.6%) in low iron deposition regions of the equatorial Pacific and Southern Ocean, and seasonally in the tropical Indian Ocean and south Pacific.

Correspondence between elevated ϕ_{sat} and low iron conditions was anticipated *a priori* because of the functional definition of fluorescence quantum yields and known responses of phytoplankton to iron stress. Recall from Eqs. (1) and (2) above that ϕ is defined as the quantum yield for light harvested by all PSI and PSII pigments, not just by the PSII complexes from which fluorescence emanates. This definition reflects the fact that PSII and PSI pigments are not distinguished in the field or from space. Consequently, ϕ is directly affected by physiological adjustments in PSII:PSI stoichiometry. Importantly, iron stress is a key environmental factor influencing PSII:PSI ratios in natural phytoplankton populations. Under low iron conditions, phytoplankton increase PSII:PSI by a factor of 2.5 to 4.0 (Sandmann, 1985; Vassiliev et al., 1995; Ivanov et al., 2000; Strzepek and Harrison, 2004). This response has been suggested as an adaptive strategy in phytoplankton for balancing ATP supplies with demand (Behrenfeld et al. 2008), and its effect is to increase pigment-specific fluorescence yields (ϕ_{sat}) in proportion to the change in PSII:PSI (Fig. 3c). In addition to these reaction center stoichiometric effects, iron-stress in the presence of elevated macronutrients (i.e., HNLC conditions) also leads to an over expression of pigment-protein complexes relative to reaction center density (Behrenfeld et al., 2006b). This response indicates a regula-

tory role for macronutrients in signaling synthetic pathways for light harvesting components. The resultant 'disassociated' antennae complexes enhance chlorophyll-specific fluorescence emission, which is reflected in elevated ϕ_{sat} values and has been used in the field to map distributions of iron-stressed phytoplankton populations (Behrenfeld et al., 2006b).

The physiological phenomena thus described provide a mechanistic link between iron stress and fluorescence yields, but realization of this relationship may not be fully captured in comparisons of high ϕ_{sat} and low iron deposition because aeolian deposition alone is not the only factor controlling iron stress in the open ocean. Additional important factors include upwelling of iron from depth, ecosystem recycling, and biomass-dependent competition for available iron. To further investigate the link between iron stress and ϕ_{sat}, we therefore employed coupled ocean circulation-ecosystem models with active iron cycling.

3.3 Satellite fluorescence yields and model nutrient stress

Ocean circulation-ecosystem models quantify biotic and abiotic nutrient fluxes and pools in the upper ocean and provide climatological predictions of growth constraints on an appropriate scale for comparison with satellite ϕ_{sat} distributions (Fig. 5). From these models, the relative bio-availability of macro- and micro-nutrients can be evaluated and an assessment made of the most limiting environmental factor for phytoplankton growth. For our global analysis, we constructed from model results (Moore et al., 2006; Moore and Braucher, 2008) a "Growth Constraint Index" (GCI) distinguishing iron-limited waters (blue areas in Fig. 5b, e) from regions limited by macronutrients (N, P) or light (red areas in Fig. 5b, e). Resultant GCI distributions reveal a strong correspondence between elevated ϕ_{sat} (>0.6%) and model predicted locations of iron-stress (yellow pixels in Fig. 5c, f), with most mismatches occurring in the Indian Ocean and along GCI boundaries (red pixels in Fig. 5c, f). Likewise, model predicted macronutrient- or light-limited waters are typically associated with low ϕ_{sat} values, such as across the Atlantic where the GCI indicates a general absence of iron-stress. Rec-

ognizing the spatial (satellite=9 km at equator; model=3.6° longitudinal, >1° latitudinal) and temporal (satellite=single season; model=climatology) inconsistencies between these data sources, this agreement of satellite observations and model predictions is rather remarkable.

The global ϕ_{sat}-model comparison presented in Fig. 5 provides strong evidence that iron-stress is an important physiological factor regulating fluorescence yields. In the Indian Ocean, however, the global model predicts that phytoplankton growth is uniformly limited by macronutrients, while elevated ϕ_{sat} values in the region suggest an occurrence of iron stress. High ϕ_{sat} values in the Indian Ocean are particularly prominent during summer, extending nearly the full width of the south-tropical basin and continuing northward along the Somali coast (Fig. 6a). To investigate this feature further, we constructed GCI distributions from a second, higher-resolution coupled model developed specifically for the Indian Ocean (Wiggert et al., 2006, 2007) that better captures upwelling processes in the region. This model predicts that macronutrients (N) limit surface phytoplankton growth in the northern Indian Ocean outside of prominent upwelling areas (red areas in Fig. 6b), while iron emerges as the most limiting nutrient in south-tropical and western regions (blue areas in Fig. 6b) (Wiggert et al., 2006, 2007). Using these model results, we again find an excellent agreement between elevated ϕ_{sat} values and model predicted iron-stress regions (Fig. 6c). If this result is upheld by future field studies, then satellite fluorescence measurements will have provided the first synoptic observational evidence that iron plays an important role in the seasonal phytoplankton dynamics of this broad, yet sparsely sampled, ocean region.[1]

[1]Recent results from field bottle-enrichment experiments evidence an occurrence of iron stress in the Arabian Sea (Moffett, J. W., Naqvi, S. W. A., Gaum, M., and Valavala, D.: Ocean Sciences Meeting Abstract, Orlando Florida, 2008).

4 The satellite fluorescence era: conclusions and future directions

Climate variability strongly impacts ocean phytoplankton productivity through its influence on the surface-layer light environment, subsurface nutrient supplies, and the aeolian flux of iron-laden dust (Behrenfeld et al., 2006a; Schneider et al., 2008). These climate-driven changes in ocean biology can be equally expressed as changes in phytoplankton biomass or physiology (Behrenfeld et al., 2008), but global-scale physiological changes elude traditional field or remote sensing approaches. Indeed, even surface nutrient inventories (e.g., Fig. 4b, c) require decades of field measurements to assemble, obfuscating climate-biology interactions functioning on shorter time-scales (e.g., El Nino – La Nina fluctuations). Phytoplankton chlorophyll fluorescence is a rich source of physiological information long exploited in the laboratory and field, and now extended to the global scale. Our results document the broad expression of key factors influencing chlorophyll fluorescence distributions that are related to phytoplankton light use efficiencies and can be compared to local observations and mechanistic models. More importantly, the satellite fluorescence record presents an opportunity to investigate how physiological properties are changing and to resolve their linkages to upper-ocean growth conditions and climate.

Iron supply to the open ocean is increasingly recognized as one of the crucial links between climate and ocean biology, functioning on short- to geologic time scales (Martin, 1990; Martin et al., 1991). Evidence of iron's important role has expanded from simple bottle experiments (e.g., Martin and Fitzwater, 1988; Martin et al., 1991, 1994; Fitzwater et al., 1996), to kilometer-scale in situ enrichments (e.g., Martin et al., 1994; Coale et al., 1996, Boyd et al., 2000; Tsuda et al., 2003; Boyd et al., 2007), to basin-scale diagnostic studies (Behrenfeld and Kolber, 1999; Behrenfeld et al., 2006B), and now to continuous global-scale assessments through satellite fluorescence. Correspondences reported here between elevated ϕ_{sat} values, low aeolian iron deposition, and model predictions of iron limitation provide compelling evidence for this new iron-stress detection capability. As an iron-stress index, ϕ_{sat} distributions offer a unique

opportunity to evaluate model predictions of nutrient limitation (e.g., Fig. 5, 6), uncover new ocean regions of iron-stress (Fig. 6), and improve ocean productivity estimates through the separate parameterization of light use efficiencies for iron-limited versus non-iron-limited populations (e.g., Behrenfeld et al., 2006b). Observations of ϕ_{sat} also provide a new tool for detecting phytoplankton responses to natural iron deposition events or even to appraise phytoplankton responses to purposeful iron injections.

Although results presented here represent a forward step in the long-standing quest to globally characterize physiological constraints on phytoplankton growth, additional advances await further investigations of fluorescence variability. For example, while we find that elevated ϕ_{sat} values are associated with low-iron conditions and that regions of macronutrient limitation are typically associated with low ϕ_{sat} values, we do not find that all predicted iron-limited waters have high ϕ_{sat}. These discrepancies are identified in Fig. 5c and f by dark blue pixels. In some cases, these mismatches represent errors in nutrient stress predictions of the model, particularly in waters where both macronutrients and iron are at the threshold of limitation. In other cases, however, low ϕ_{sat} values are found in waters well established as iron limited, such as the subarctic north Pacific and highest latitudes of the Southern Ocean (Fig. 5) (Boyd et al., 2007). Such occurrences can be attributed to additional physiological factors influencing fluorescence yields.

One factor that is particularly influential on satellite-derived fluorescence yields is NPQ. In the current treatment, a simple inverse-light function has been applied for the NPQ correction. While such a relationship may be appropriate for phytoplankton acclimated to a single light level (Fig. 2c, 3a, b) and is consistent to first-order with our satellite data (Fig. 2d), the actual reduction in ϕ_{sat} from NPQ expressed at any given saturating *iPAR* differs between phytoplankton acclimated to different light levels (Fig. 3d). Specifically, low-light acclimated phytoplankton dissipate a greater fraction of absorbed light energy as heat than high-light acclimated phytoplankton exposed to the same saturating light level (Fig. 3d). Importantly, mixed layer light levels (i.e., the light level to which phytoplankton photoacclimate) are typically lower at high latitudes

than nearer the equator. Applying a single inverse-light function at all latitudes, therefore, will tend to over-correct for NPQ at high latitudes, yielding dampened ϕ_{sat} values. This consideration alone may account for the general absence of elevated ϕ_{sat} in the high-latitude, iron-limited waters of the subarctic Pacific and Southern Ocean (Fig. 5). Addressing this issue represents an important challenge for future satellite fluorescence analyses and will require the description of NPQ as a function of both *iPAR* and photoacclimation state. In the current study, we have not implemented such an approach because light-acclimation responses in natural phytoplankton assemblages remain poorly-constrained and large uncertainties still exist in assessing physiologically-relevant surface mixing layer depths (required for calculating mixed layer acclimation light levels).

In addition to photoacclimation-dependent variability in the ϕ-*iPAR* relationship, other factors must also be considered in future interpretations of global ϕ_{sat} distributions. For example, non-steady-state growth conditions (particularly the onset of nutrient stress) appear to result in transient modulations in fluorescence quantum yields (Schallenberg et al., 2008). Taxonomic factors may also require consideration, particularly with respect to their influence on ϕ_{sat} through changes in accessory pigments or PSII:PSI responses to iron-stress. As these remaining issues are resolved, we can anticipate new insights on phytoplankton physiology and ecology to emerge from the satellite chlorophyll fluorescence record, as well as an independent global data set for regionally- and globally evaluating satellite chlorophyll retrieval algorithms (e.g., *Fig. A2*).

Appendix A

A1 Derivation of fluorescence quantum yield from space

In the following subsections, we describe the stepwise treatment of the fluorescence signal as measured with NASA's MODIS sensor on Aqua that culminates in a phytoplankton fluorescence quantum yield accounting for effects of pigment packaging and non-photochemical quenching.

A2 Satellite ocean color measurement of chlorophyll fluorescence

Satellite measurements of chlorophyll fluorescence from the MODIS sensor, F_{sat}, are derived from determinations of the normalized water leaving radiance, $L_{WN}(\lambda)$ (e.g., Abbott and Letelier, 1999). Values of $L_{WN}(\lambda)$ (a level 2 data product from NASA's processing stream; http://oceancolor.gsfc.nasa.gov/PRODUCTS) is related to the water leaving radiance ($L_W(\lambda)$):

$$L_{WN}(\lambda)=L_W(\lambda)\frac{F_0(\lambda)}{E_d(0^+,\lambda)}, \tag{A1}$$

where $E_d(0^+,\lambda)$ is downwelling irradiance just above the surface, and $F_0(\lambda)$ is the solar irradiance spectrum at the top of the atmosphere (Gordon and Voss, 1999). Near the peak of chlorophyll fluorescence emission, three processes contribute to water leaving radiance: $L_W(678)$, elastic backscattering of light, Raman scattering by water, and chlorophyll fluorescence (e.g., Kiefer et al., 1989; Westberry and Siegel, 2003). To obtain the chlorophyll fluorescence signal from ocean color remote sensing, a line height calculation is performed that removes effects of backscattering and Raman scattering (Abbott and Letelier, 1999):

$$F_{\text{sat}}=L_{WN}(678)-\frac{70}{81}L_{WN}(667)-\frac{11}{81}L_{WN}(748), \tag{A2}$$

where $L_{wN}(\lambda)$ are the water leaving radiances at the respective wavelengths in units of $mW\,cm^{-2}\,sr^{-1}\,\mu m^{-1}$. F_{sat}, also called fluorescence line height, is currently a MODIS level-3 evaluation product (http://oceancolor.gsfc.nasa.gov/cgi/l3). Fluoresced radiance $L_{W,f}(0^+, 678)$ is equal to:

$$L_{W,f}(0^+, 678) = F_{sat}\frac{E_d(0^+, 678)}{F_0(678)}, \quad \text{(A3)}$$

where $F_0(678)$ is 148.097 $mW\,cm^{-2}\,\mu m^{-1}$ (Thuillier et al., 2003).

A3 Fluorescence radiance emanating from the oceans

The contribution of fluoresced radiance at the detected emission band (λ_{em}) from a subsurface layer between z_1 and $z_1+\Delta z$ and measured at the emission band is equal to:

$$\Delta L_{W,f}(\lambda_{em}, z_1, \Delta z) = \frac{\varphi}{4\pi C_f}\int_{z_1+\Delta z}^{z_1}\int_{400}^{700}\frac{\lambda}{hc}a_{ph}(\lambda, z)E_0(0^-, \lambda)e^{-K(\lambda,z)z}d\lambda dz, \quad \text{(A4)}$$

where the integral with respect to depth accounts for the loss of light energy with depth at a rate equal to the diffuse attenuation coefficient $K(\lambda,z)(m^{-1})$ and absorbed by phytoplankton with an absorption coefficient $a_{ph}(\lambda,z)(m^{-1})$. In Eq. (A4) the 4π factor accounts for the fact that fluorescence is isotropic, C_f is the inverse proportion of photons fluoresced at the detected emission waveband around λ_{em} relative to the full fluorescence spectrum (nm), φ is the quantum yield of fluorescence (total number of fluoresced photons per absorbed photons), $E_0(0^-, \lambda)$ is the scalar irradiance ($W\,m^{-2}\,nm^{-1}$), and the factor, λ/hc, translates $E_0(0^-, \lambda)$ into units of quanta $m^{-2}\,nm^{-1}$ (e.g., Kiefer et al., 1989; Huot et al., 2005). The units of $\Delta L_{w,f}(\lambda_{em}, z_1)$ are thus quanta $m^{-2}\,nm^{-1}\,sr^{-1}$.

We next assume an optically homogeneous upper ocean in terms of the phytoplankton absorption coefficient and diffuse attenuation coefficients. This assumption introduces little error because remotely detected fluorescence is dominated by the upper

several meters of the ocean and measured with the sun near its highest position in the sky. We also neglect reabsorption of fluoresced light within the emitting phytoplankton (e.g., Collins et al., 1985), which is valid for $Chl<2\,\mathrm{mg\,m^{-3}}$ (Fig. 1 in Huot et al., 2005).

Fluoresced light is attenuated on its way to the surface with a diffuse attenuation coefficient $k_L(\lambda_{em})$. Integrating over all depths z contributing to fluoresced light (e.g. Huot et al., 2005), we get:

$$L_{w,f}(\lambda_{em},0^-)=\frac{\varphi}{4\pi C_f}\int_{400}^{700}\frac{\lambda}{hc}\frac{1}{(K(\lambda)+k_L(\lambda_{em}))}a_{\mathrm{ph}}(\lambda)E_0(0^-,\lambda)d\lambda. \quad \text{(A5)}$$

The fluoresced water-leaving radiance, $L_{w,f}(\lambda_{em},0^+)$, is equal to the fluoresced radiance just beneath the sea surface, $L_{w,f}(\lambda_{em},0^-)$, transmitted across the air-sea interface:

$$L_{w,f}(\lambda_{em},0^+)=\frac{tL_{w,f}(\lambda_{em},0^-)}{n_w^2}=0.546L_{w,f}(\lambda_{em},0^-), \quad \text{(A6)}$$

where n_w is the index of refraction of sea water (n_w=1.34) and t is the transmission of nadir radiance across the sea surface (t=0.97; Mobley, 1994).

A4 Quantum yield determination

Combining (A5) and (A6), equating it with (A3) at the emission wavelength (678 nm), and solving for the quantum yield, we get:

$$\varphi=\frac{4\pi n_w^2 C_f}{tF_0(678)}\frac{E_d(678,0^+)F_{\mathrm{sat}}}{\int_{400}^{700}\frac{\lambda}{hc}\frac{1}{(K(\lambda)+k_L(678))}a_{\mathrm{ph}}(\lambda)E_0(0^-,\lambda)d\lambda}= \quad \text{(A7)}$$

$$\frac{6.8E_d(678,0^+)F_{\mathrm{sat}}}{\int_{400}^{700}\frac{\lambda}{hc}\frac{1}{(K(\lambda)+k_L(678))}a_{\mathrm{ph}}(\lambda)E_0(0^-,\lambda)d\lambda},$$

where C_f=43.38 nm for MODIS (Huot et al., 2005).

A series of approximations are then applied to solve (A7) for the quantum yield. First we convert the scalar irradiance back to units of W m^{-2} nm^{-1}:

$$\varphi = \frac{6.8 E_d(678, 0^+) F_{\text{sat}}}{\int_{400}^{700} \frac{1}{(K(\lambda)+k_L(678))} a_{\text{ph}}(\lambda) E_0(0^-, \lambda) d\lambda} \quad \text{(A8)}$$

Total light attenuation is then estimated using the dominating attenuation of the upwelling fluoresced light by water ($k_L(678) \sim a_w(678) = 0.46\,\text{m}^{-1}$) and the smaller contribution by the attenuation of downwelling light (valid for $Chl < 2\,\text{mg m}^{-3}$, Kiefer et al., 1989):

$$K(\lambda) + k_L(678) \approx 0.52\,\text{m}^{-1} \quad \text{(A9)}$$

Approximating the solar excitation spectrum as spectrally flat, scalar irradiance as $E_d(\lambda) = 0.87 E_0(\lambda)$ (e.g., Westberry and Siegel, 2003), and adding one air-sea interface crossing (t=0.97):

$$\text{tE}_\text{d}(678, 0^+) = 0.84\,\text{E}_0(678, 0^-) = 0.84 \frac{\int_{400}^{700} \text{E}_0(\lambda, 0^-) \text{d}\lambda}{300\,\text{nm}} \quad \text{(A10)}$$

$$\rightarrow \frac{E_d(678, 0^+)}{\int_{400}^{700} E_0(\lambda, 0^-) d\lambda} = 0.003\,\text{nm}^{-1}.$$

Finally, substituting (A9) and (A10) into (A8), the quantum yield (no units) becomes:

$$\varphi = 0.01 \frac{F_{\text{sat}}}{<a_{\text{ph}}>}, \quad \text{(A11)}$$

where $<a_{\text{ph}}>$ is the spectrally-averaged phytoplankton absorption coefficient (m^{-1}). The constant 0.01 is equal to the inverse of the constant S in Eq. (2) of the main article, where S is approximated at 100 mW cm^{-2} μm^{-1} sr^{-1} m.

The term $<a_{ph}>$ is estimated using satellite determinations of chlorophyll concentration, Chl_{sat}, using published relationships between $a_{ph}(\lambda)$ and Chl integrated spectrally over the primary photosynthetic absorption band of 400 to 530 nm (Bricaud et al., 1998):

$$<a_{ph}>=0.027 Chl_{sat}^{0.657}. \quad \text{(A12)}$$

This formulation takes into account phytoplankton pigment packaging and corresponds to a spectrally integrated, chlorophyll-specific absorption spectrum of:

$$<a^*_{ph}>=0.027 Chl_{sat}^{-0.343}. \quad \text{(A13)}$$

Combining equations (A11) and (A12) yields a satellite-based estimate of φ corrected for pigment packaging:

$$\varphi=0.37 F_{sat} Chl_{sat}^{-0.657}. \quad \text{(A14)}$$

Correction of the satellite fluorescence for effects of non-photochemical quenching (NPQ) is acheived by using a $1/iPAR$ relationship normalized to the average $iPAR$ value for the MODIS record ($\overline{iPAR}$=1590 μmole photons m^{-2} s^{-1}) (e.g., Morrison, 2003; Figs. 2c and 3a, b). Hence: *NPQ-corrected* $F_{sat}=F_{sat}\, iPAR/\overline{iPAR}$.

Combining this NPQ correction with Eq. (A14), we get an NPQ and pigment packaging corrected satellite fluorescence quantum yield (φ_{sat}) of:

$$\varphi_{sat}=0.37\frac{F_{SAT}}{Chl_{sat}^{0.657}}\frac{iPAR}{\overline{iPAR}}=0.00024\frac{F_{sat} iPAR}{Chl_{sat}^{0.657}}. \quad \text{(A15)}$$

Equation (A15) enables φ_{sat} values to be determined from satellite determinations of F_{sat}, $iPAR$ and Chl_{sat}. Chlorophyll estimates, Chl_{sat}, are from the standard NASA algorithm (OC-3), while MODIS iPar is based on Carder et al. (2003).

The focus of the current manuscript is the characterization of phytoplankton physiological variability, but this is not the only valuable application of satellite fluorescence

data. As illustrated in Fig. 2e and f, global variability in fluorescence quantum yields is highly constrained relative to variability in chlorophyll concentration (e.g., Fig. 1b). Accordingly, correction of fluorescence data for primary factors contributing to quantum yield variations (e.g., Eq. A15) yields products that could be used to evaluate regional biases in satellite chlorophyll products from the alternative empirical- and semi-analytic algorithms based on measurement bands in the blue-green spectral region (e.g., Fig. A2).

Acknowledgements. This work was supported by grants from the NASA Ocean Biology and Biogeochemistry Program and the NSF Biological Oceanography Program.

References

Abbott, M. R. and Letelier, R. M.: Algorithm theoretical basis document chlorophyll fluorescence (MODIS product number 20). NASA, 1999.

Ahn, Y.-H. and Shanmugam, P.: Derivation and analysis of the fluorescence algorithms to etimate phytoplankton pigment concentration in optically complex coastal waters, J. Opt. A: Pure Appl. Opt., 9, 352–362, 2007.

Behrenfeld, M. J. and Kolber, Z. S.: Widespread iron limitation of phytoplankton in the south Pacific ocean, Science, 283, 840–843, 1999.

Behrenfeld, M. J. Randerson, J. T., McClain, C. R., Feldman, G. C., Los, S., Tucker, C., Falkowski, P. G., Field, C. B., Frouin, R., Esaias, W., Kolber, D., and Pollack, N.: Biospheric primary production during an ENSO transition, Science, 291, 2594–2597, 2001.

Behrenfeld, M. J., Boss, E. S., Siegel, D. A., and Shea, D. M.: Carbon-based ocean productivity and phytoplankton physiology from space, Global Biogeochem. Cy., 19, GB1006, doi:10.1029/2004GB002299, 2005.

Behrenfeld, M. J., O'Malley, R., Siegel, D. A., McClain, C. R., Sarmiento, J. L., Feldman, G. C., Milligan, A. J., Falkowski, P. G., Letelier, R., and Boss, E. S.: Climate-driven trends in contemporary ocean productivity, Nature, 444, 752–755, 2006a.

Behrenfeld, M. J., Worthington, K., Sherrell, R. M., Chavez, F. P., Strutton, P., McPhaden, M., and Shea, D. M.: Controls on tropical Pacific Ocean productivity revealed through nutrient stress diagnostics, Nature, 442, 1025–1028, 2006b.

Behrenfeld, M. J., Halsey, K., and Milligan, A. J.: Evolved physiological responses of phytoplankton to their integrated growth environment, Phil. Trans. Royal Soc. B, 363, doi:10.1098/rstb.2008.0019, 2008.
Boyd, P. W., Watson, A. J., Law, C. S., et al.: A mesoscale phytoplankton bloom in the polar Southern ocean stimulated by iron fertilization, Nature, 407, 695–702, 2000.
Boyd, P., Juckells, T., Law, C. S., et al.: Mesoscale iron enrichment experiments 1993–2005: Synthesis and future directions, Science, 315, 612–617, 2007.
Bricaud, A., Babin, M., Morel, A., and Claustre, H.: Variability in the chlorophyll-specific absorption coefficients for natural phytoplankton: Analysis and parameterization, J. Geophys. Res., 100, 13 321–13 332, 1995.
Bricaud, A., Morel, A., Babin, M., Allalli, K., and Claustre, H.: Variations of light absorption by suspended particles with chlorophyll a concentration in oceanic (case 1) waters: Analysis and implications for bio-optical models, J. Geophys. Res, 103, 31 033–31 044, 1998.
Coale, K., Johnson, K. S., Fitzwater, S. E., et al.: A massive phytoplankton bloom induced by an ecosystem-scale iron fertilization experiment in the equatorial Pacific ocean, Nature, 383, 495–501, 1996.
Duysens, L. N. M.: The flattening of the absorption spectra of suspensions as compared to that of solutions, Biochim. Biophys. Acta, 19, 1–12, 1956.
Falkowski, P. G. and Kiefer, D. A.: Chlorophyll a fluorescence in phytoplankton: Relationship to photosynthesis and biomass, J. Plankton Res., 7, 715–731, 1985.
Falkowski, P. G. and Kolber, Z.: Variations in chlorophyll fluorescence yields in phytoplankton in the world oceans, Austral. J. Plant Physiol., 22, 341–355, 1995.
Field, C. B., Behrenfeld, M. J., Randerson, J. T., and Falkowski, P. G.: Primary production of the biosphere: Integrating terrestrial and oceanic components, Science, 281, 237–240, 1998.
Fitzwater, S. E., Coale, K. H., Gordon, R. M., Johnson, K. S., and Ondrusek, M. E.: Iron deficiency and phytoplankton growth in the equatorial Pacific, Deep Sea Res. II, 43, 995–1015, 1996.
Garcia, H. E., Locarnini, R. A., Boyer, T. P., and Antonov, J. I.: World Ocean Atlas 2005, Volume 4, Nutrients (phosphate, nitrate, silicate), in: S. Levitus [ed.], NOAA Atlas NESDIS 64, US Government Printing Office, Washington, D.C., 396 pp., 2006.
Gilerson, A., Zhou, J., Hlaing, S., Ioannou, I., Schalles, J., Gross, B., Moshary, F., and Ahmed, S.: Fluorescence component in the reflectance spectra from coastal waters. Dependence on water composition, Opt. Express, 15, 15 702–15 720, 2007.

Gilerson, A., Zhou, J., Hlaing, S., Ioannou, I., Gross, B., Moshary, F., and Ahmed, S.: Fluorescence component in the reflectance spectra from coastal waters. II. Performance of retrieval algorithms, Opt. Express, 16, 2446–2460, 2008.
Gower, J. F. R., Brown, L., and Borstad, G. A.: Observation of chlorophyll fluorescence in west coast waters of Canada using the MODIS satellite sensor, Can. J. Remote Sensing, 30, 17–25, 2004.
Gower, J. F. R. and King, S.: Validation of chlorophyll fluorescence derived from MERIS on the west coast of Canada, Int. J. Remote Sens., 28, 625–635, 2007.
Hu, C., Muller-Karger, F. E., Taylor, C. J., Carder, K. L., Kelble, C., Johns, E., and Heil, C. A.: Red tide detection and tracing using MODIS fluorescence data: A regional example in SW Florida coastal waters, Remote Sens. Environ., 97, 311–321, 2005.
Huot, Y., Brown, C. A., and Cullen, J. J.: New algorithms for MODIS sun-induced chlorophyll fluorescence and a comparison with present data products, Limnol. Oceanogr., 3, 108–130, 2005.
Huot, Y., Brown, C. A., and Cullen, J. J.: Retrieval of phytoplankton biomass from simultaneous inversion of reflectance, the diffuse attenuation coefficient, and sun-induced fluorescence in coastal waters, J. Geophys. Res., 112, C06013, doi:10.1029/2006JC003794, 2007.
Ivanov, A. G., Park, Y.-I., Miskiewicz, E., Raven, J. A., Huner, N. P. A., and Öquist, G.: Iron stress restricts photosynthetic intersystem electron transport in Synechococcus sp. PCC 7942, FEBS Lett., 485, 173–177, 2000.
Kiefer, D. A., Chamberlin, W. S. and Booth, C. R.: Natural fluorescence of chlorophyll a: Relationship to photosynthesis and chlorophyll concentration in the western South Pacific gyre, Limnol. Oceanogr., 34, 868–881, 1989.
Kistler, R., Kalnay, E., Collins, W., et al.: The NCEP-NCAR 50-year reanalysis: Monthly means CD-ROM and documentation, B. Am. Meteorol. Soc., 82, 247–267, 2001.
Krause, G. H. and Weis, E.: Chlorophyll fluorescence and photosynthesis: the basics, Ann. Rev. Plant Physiol. Plant Molec. Biol., 42, 313–349, 1991.
Letelier, R. M., Abbott, M. R. and Karl, D. M.: Chlorophyll natural fluorescence response to upwelling events in the Southern Ocean, Geophys. Res. Lett., 24, 409–412, 1997.
Luo, C., Mahowald, N., and Corral, J. D.: Sensitivity study of meteorological parameters on mineral aerosol mobilization, transport and distribution, J. Geophys. Res., 108, 4447, doi:10.1029/2003JD0003483, 2003.
Luo, C., Mahowald, N. M., Meskhidze, N., et al.: Estimation of iron solubility from observations

and a global aerosol model, J. Geophys. Res., 110, D23307, doi:10.1029/2005JD006059, 2005.
Luo, C., Mahowald, N. M., Bond, T., et al.: Combustion iron distribution and deposition, Global Biogeochem. Cy., 22, doi:10.1029/2007GB002964, 2008.
Mahowald, N., Luo, C., Corral, J. D., and Zender, C.: Interannual variability in atmospheric mineral aerosols from a 22-year model simulation and observational data, J. Geophys. Res., 108, 4352, doi:10.1029/2002JD002821, 2003.
Martin, J. H. and Fitzwater, S. E.: Iron deficiency limits phytoplankton growth in the north-east Pacific subarctic, 331, 341–343, 1988.
Martin, J. H.: Glacial-interglacial CO_2 change: The iron hypothesis, Paleoceanography, 5, 1–13, 1990.
Martin, J. H., Gordon, R. M., and Fitzwater, S. E.: The case for iron, Limnol. Oceanogr., 36, 1793–1802, 1991.
Martin, J. H., Coale, K., Johnson, K. S., et al.: Testing the iron hypothesis in ecosystems of the equatorial Pacific ocean, Nature, 371, 123–129, 1994.
Moore, J. K. and Braucher, O.: Sedimentary and mineral dust sources of dissolved iron to the world ocean, Biogeosciences, 5, 631–656, 2008, http://www.biogeosciences.net/5/631/2008/.
Moore, J. K., Doney, S. C., Lindsay, K., Mahowald, N., and Michaels, A. F.: Nitrogen fixation amplifies the ocean biogeochemical response to decadal timescale variations in mineral dust deposition, Tellus, 58B, 560–572, 2006.
Morel, A. and Prieur, L.: Analysis of variations in ocean color, Limnol. Oceanogr., 22, 709–722, 1977.
Morrison, J. R.: In situ determination of the quantum yield of phytoplankton chlorophyll fluorescence: A simple algorithm, observations, and model, Limnol. Oceanogr., 48, 618–631, 2003.
Müller, P., Li, X.-P., and Niyogi, K. N.: Non-photochemical quenching. A response to excess light energy, Plant Physiol., 125, 1558–1566, 2001.
Neville, R. A. and Gower, J. F. R.: Passive remote sensing of phytoplankton via chlorophyll a fluorescence, J. Geophys. Res., 82, 3487–3493, 1977.
Sandmann, G.: Consequences of iron deficiency on photosynthetic and respiratory electron transport in blue-green algae, Photosyn. Res., 6, 261–271, 1985.
Schallenberg, C., Lewis, M. R., Kelley, D. E., and Cullen, J. J.: Inferred influence of nutrient

availability on the relationship between Sun-induced chlorophyll fluorescence and incident irradiance in the Bering Sea, J. Geophys. Res., 113, C07046, doi:10.1029/2007JC004355, 2008.

Schneider, B., Bopp, L., Gehlen, M., Segschneider, J., Frölicher, T. L., Cadule, P., Friedlingstein, P., Doney, S. C., Behrenfeld, M. J., and Joos, F.: Climate-induced interannual variability of marine primary and export production in three global coupled climate carbon cycle models, Biogeosciences, 5, 597–614, 2008, http://www.biogeosciences.net/5/597/2008/.

Strzepek, R. F. and Harrison, P. J.: Photosynthetic architecture differs in coastal and oceanic diatoms, Nature, 43, 689–692, 2004.

Topliss, B. J. and Platt, T.: Passive fluorescence and photosynthesis in the ocean: implications for remote sensing, Deep-Sea Res., 33, 849–864, 1986.

Tsuda, A., Takeda, S., Saito, H., et al.: A mesoscale iron enrichment in the western Subarctic Pacific induces a large centric diatom bloom, Science, 300, 958–961, 2003.

Vassiliev, I. R., Kolber, Z., Wyman, K. D. et al.: Effects of iron limitation on photosystem II composition and light utilization in *Duneliella tertiolecta*, Plant Physiol., 109, 963–972, 1995.

Wagener, T., Guieu, C., Losno, R., Bonnet, S., and Mahowald, N.: Revisiting atmospheric dust export to the Southern Ocean: Biogeochemical implications, Global Biogeochem. Cy., 22, doi:10.1029/2007GB002984, 2008.

Wiggert, J. D., Murtugudde, R. G., and Christian, J. R.: Annual ecosystem variability in the tropical Indian Ocean: Results from a coupled bio-physical ocean general circulation model, Deep-Sea Res. II, 53, 644–676, 2006.

Wiggert, J. D. and Murtugudde, R. G.: The sensitivity of the southwest monsoon phytoplankton bloom to variations in aeolian iron deposition over the Arabian Sea, J. Geophys. Res., 112, doi:10.1029/2006JC003514, 2007.

Zender, C., Bian, H., and Newman, D.: Mineral dust entrainment and deposition (DEAD) model: Description and 1990s dust climatology, J. Geophys. Res., 108, 4416, doi:10.1029/2002JD002775, 2003.

References to Appendix figures

Abbott, M. R. and Letelier, R. M.: Algorithm theoretical basis document chlorophyll fluorescence (MODIS product number 20, online available at: http://modis.gsfc.nasa.gov/data/atbd/atbd_

mod22.pdf), NASA, 1999.
Bricaud, A., Morel, A., Babin, M., Allalli, K., Claustre, H.: Variations of light absorption by suspended particles with chlorophyll a concentration in oceanic (case 1) waters: Analysis and implications for bio-optical models. J. Geophys. Res. 103, 31 033–31 044, 1998.
Carder, K. L., Chen, R., and Hawes, S.: Algorithm theoretical basis document ATBD 20: Instantaneous photosynthetically available radiation and absorbed radiation by phytoplankton. (version 7, online available at: http://modis.gsfc.nasa.gov/data/atbd/atbd_mod20.pdf), NASA, 2003.
Collins, D. J., Kiefer, D. A., Soohoo, J. B., and McDermid, I. S.: The role of reabsorption in the spectral distribution of phytoplankton fluorescence emission, Deep-Sea Res., 32, 983–1003, 1985.
Gordon, H. R. and Voss, K. J.: Algorithm theoretical basis document normalized Water leaving Radiance, (MOD 18, online available at: http://modis.gsfc.nasa.gov/data/atbd/atbd_mod18.pdf), NASA, 1999.
Huot, Y., Brown, C. A., and Cullen, J. J.: New algorithms for MODIS sun-induced chlorophyll fluorescence and a comparison with present data products, Limnol. Oceanogr., 3, 108–130, 2005.
Kiefer, D. A., Chamberlin, W. S., Booth, and C. R.: Natural fluorescence of chlorophyll a: Relationship to photosynthesis and chlorophyll concentration in the western South Pacific gyre, Limnol. Oceanogr. 34, 868–881, 1989.
Lee, Z. P., Carder, K. L., and Arnone, R.: Deriving inherent optical properties from water color: A multi-band quasi-analytical algorithm for optically deep waters, Appl. Opt., 41, 5755–5772, 2002.
Mobley, C. D. Light and Water: Radiative Transfer in Natural Waters, Academic Press, San Diego, California, USA, 592 pp., 1994.
Thuillier, G., Hersé, M., Simon, P. C., Labs, D., Mandel, H., Gillotay, D., and Foujols, T.: The solar spectral irradiance from 200 to 2400 nm as measured by the SOLSPEC spectrometer from the ATLAS 1-2-3 and EURECA missions, Solar Physics, 214, 1–22, 2003.
Westberry T. K. and Siegel, D. A.: Phytoplankton natural fluorescence in the Sargasso Sea: Prediction of primary production and eddy induced nutrient fluxes Deep-Sea Research, Part I, 50, 417–434, 2003.

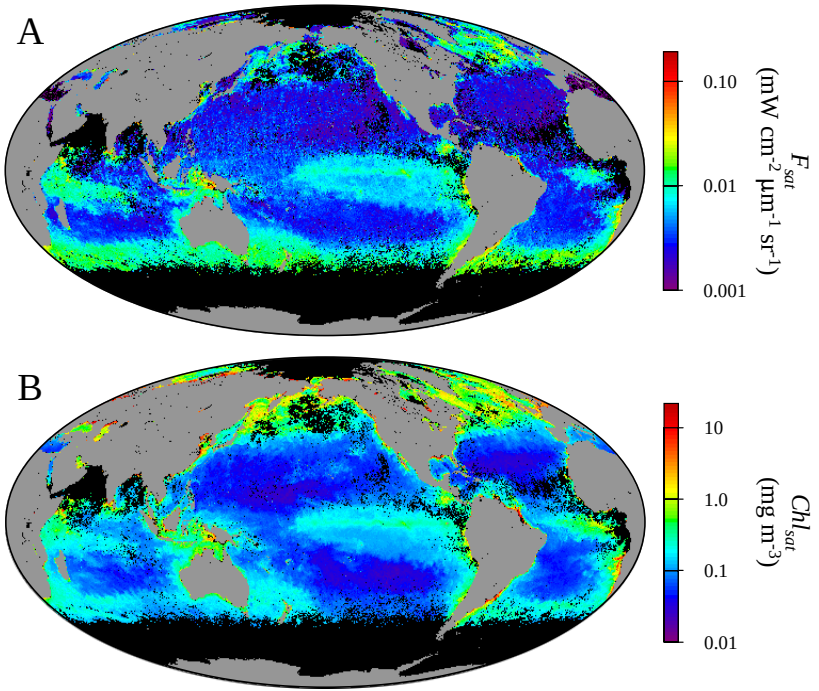

Fig. 1. July 2004 examples of global monthly average MODIS **(a)** F_{sat} and **(b)** Chl_{sat}. Chlorophyll concentrations are derived using the standard NASA algorithm (OC-3).

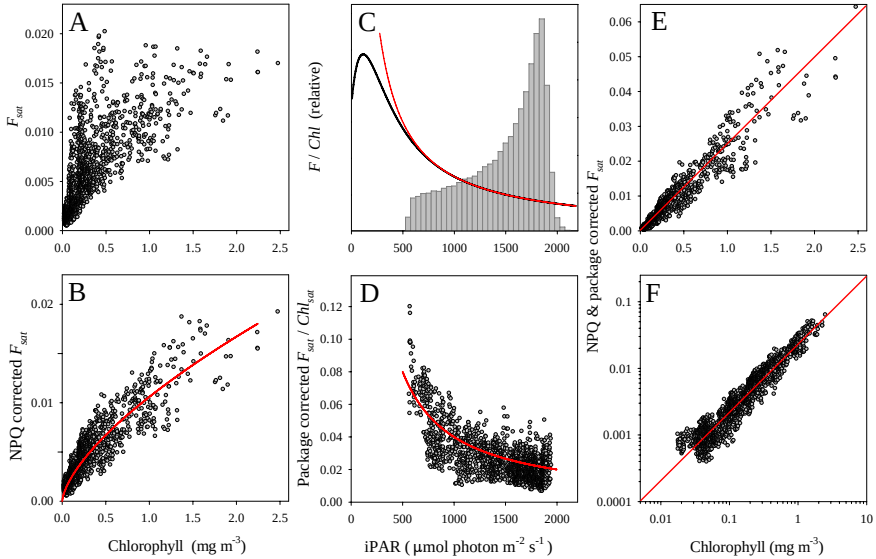

Fig. 2. Primary factors regulating global F_{sat} distributions over the 5 year MODIS record. **(a)** Relationship between binned Chl_{sat} and F_{sat} (see *Appendix A, Fig. A1* for bin designations) **(b)** Relationship between Chl_{sat} and NPQ-corrected F_{sat} ($=F_{sat}\times {}^{\overline{iPAR}}/_{iPAR}$). Curvature reflects pigment packaging effects, which closely follow published changes in $<a_{ph}>$ for the primary photosynthetic absorption band (400–530 nm) (red line) (Bricaud et al., 1998) (Appendix A). **(c)** Theoretical relationship between chlorophyll-specific fluorescence and *iPAR* (black curve) (see also text and Fig. 3). Fluorescence initially increases with light as photosynthesis saturates, then decreases at high *iPAR* in a ${}^{1}/_{iPAR}$ manner due to NPQ (red line). Gray bars show frequency histogram for MODIS *iPAR*. **(d)** Observed relationship between *iPAR* and chlorophyll-specific F_{sat} corrected for packaging effects (package correction = $<a^*_{ph}>/\overline{<a^*_{ph}>}$, where $<a^*_{ph}>=0.027\ Chl_{sat}^{-0.343}$ and $\overline{<a^*_{ph}>}$ is the value of $<a^*_{ph}>$ for the global average Chl_{sat} of 0.134 mg m^{-3}=0.0538 m^{-1}) Red line=scaled ${}^{1}/_{iPAR}$ relationship. **(e)** Relationship between Chl_{sat} and F_{sat} corrected for NPQ- and pigment packaging (r=0.96). **(f)** Same as panel e, except with log-transformed axes (see also *Appendix A, Fig. A2*). Fluorescence units for panels b, c, e, and f are mW cm^{-2} μm^{-1} sr^{-1}. Fluorescence units for panel d are mW cm^{-2} μm^{-1} sr^{-1} (mg chl m^{-3})$^{-1}$.

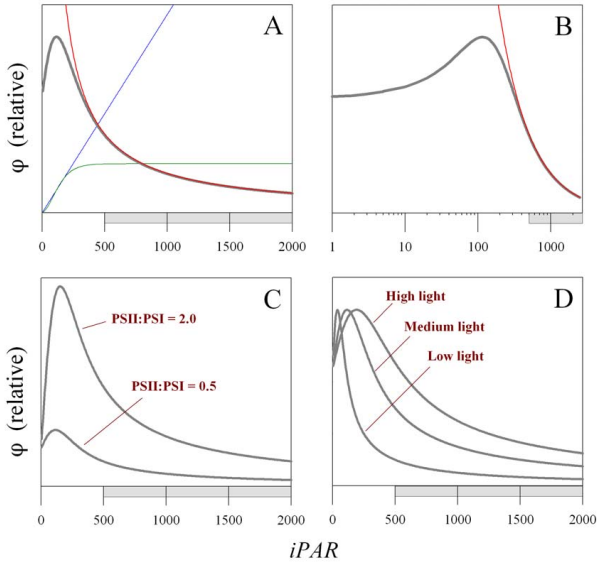

Fig. 3. Relationships between fluorescence quantum yield (ϕ) and incident light (*iPAR*). **(a)** Changes in ϕ with *iPAR* for a phytoplankton population acclimated to a single light level. Blue line=absorbed light energy (relative). Green line=fluorescence (relative). Gray line = ϕ. Red line=scaled $^{1}/_{iPAR}$ function. **(b)** Same ϕ data as in panel (a) but plotted against a log-transformed *iPAR* axis, making this plot directly comparable to Fig. 9 of Morrison (2003) and Fig. 11 of Schallenberg (2008). Red line = scaled $^{1}/_{iPAR}$ function. **(c)** Change in the ϕ-*iPAR* relationship corresponding to a PSII:PSI ratio shift from 0.5 to 2.0. **(d)** Changes in the ϕ-*iPAR* relationship resulting from photoacclimation to different light levels. Phytoplankton grown at low-light become light saturated at low *iPAR* levels and then exhibit strong NPQ upon exposure to higher *iPAR* levels (lower curve). Higher-light acclimated phytoplankton require higher light levels to saturate photosynthesis and engage NPQ (middle and upper curves). For any one of these three curves, the reduction in ϕ from NPQ at supersaturating light levels is well described by an inverse function of *iPAR*. However, the NPQ effect *at any given saturating iPAR level* is stronger in the lower-light acclimated phytoplankton than in the higher-light acclimated cells. This dependence of NPQ on photoacclimation state implies that a single, globally-applied inverse-light function will tend to under-correct for NPQ at high *iPAR* and overcompensate for NPQ at low *iPAR* if photoacclimation is positively correlated with *iPAR* (as occurs with changes in latitude). (a–d) Gray bar on x-axis indicates *iPAR* range for MODIS fluorescence measurements.

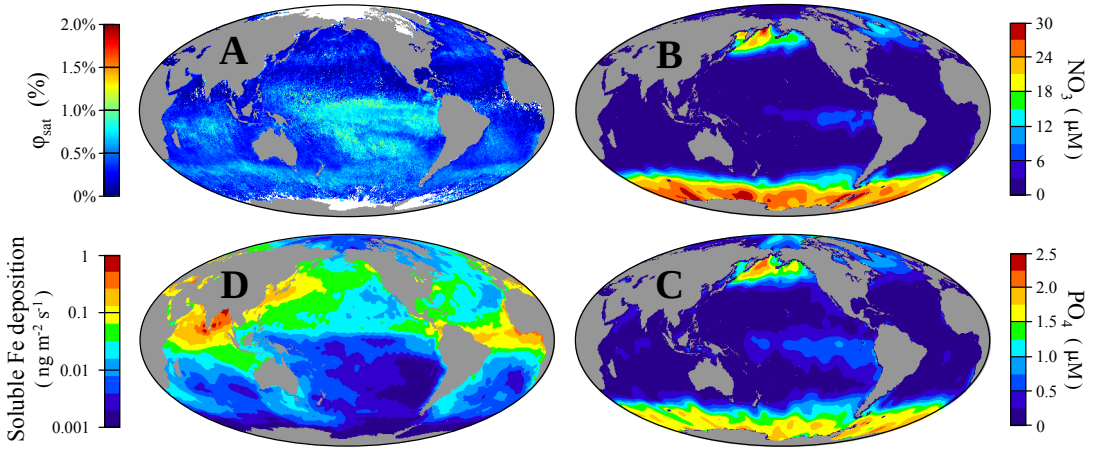

Fig. 4. Comparison of **(a)** ϕ_{sat} with **(b)** surface nitrate concentration, **(c)** surface phosphate concentration, and **(d)** aeolian soluble iron deposition. Values of ϕ_{sat} and iron deposition are for spring 2004 (March–May). NO_3 and PO_4 are World Ocean Atlas climatological spring values. White pixels in (a) indicate ice cover.

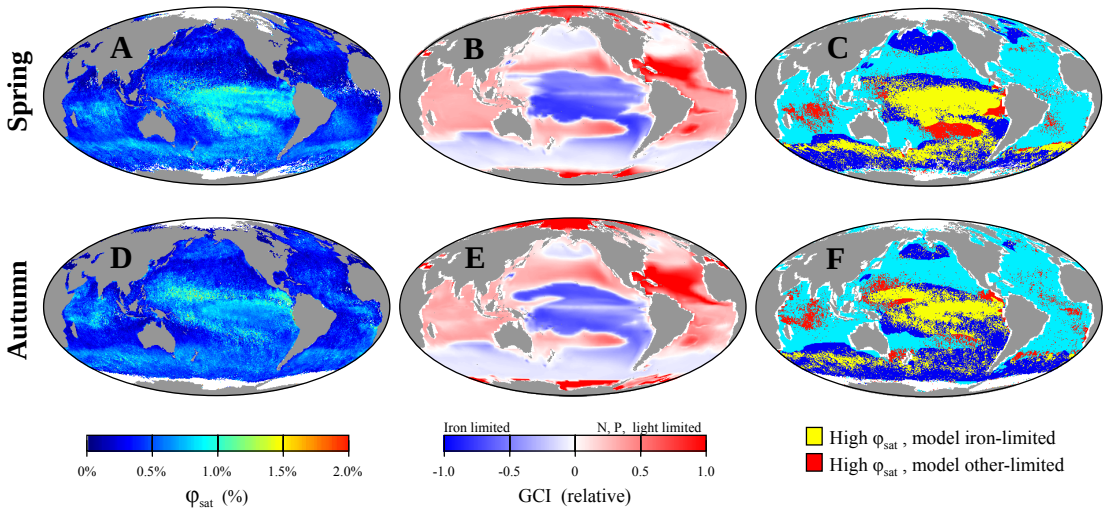

Fig. 5. Comparison of global ϕ_{sat} and model-based GCI (Moore et al., 2006) for (**a–c**) boreal spring (March–May) and (**d–f**) boreal autumn (September–November). (a, d) = ϕ_{sat}. (b, e) = GCI. The model generates a relative stress index (0 to 1) for each growth factor (iron, light, N, P). GCI is the log transform of the ratio of the iron stress index to that for the most limiting other factor (light, N, or P). Blue = GCI<0, Fe-limited. Red = GCI>0, macronutrient or light-limited. (c, f) State-space comparison of satellite and model results. (background) Dark blue = GCI<0. Light blue = GCI>0. (foreground) Yellow = high ϕ_{sat}(>0.6%) matches model iron-stress. Red=high ϕ_{sat} coincides with other model stress. Spring and autumn seasons are shown because the latitudinal distribution of light is most evenly distributed across mid- and low-latitudes during these periods, thus minimizing impacts of physiological light acclimation.

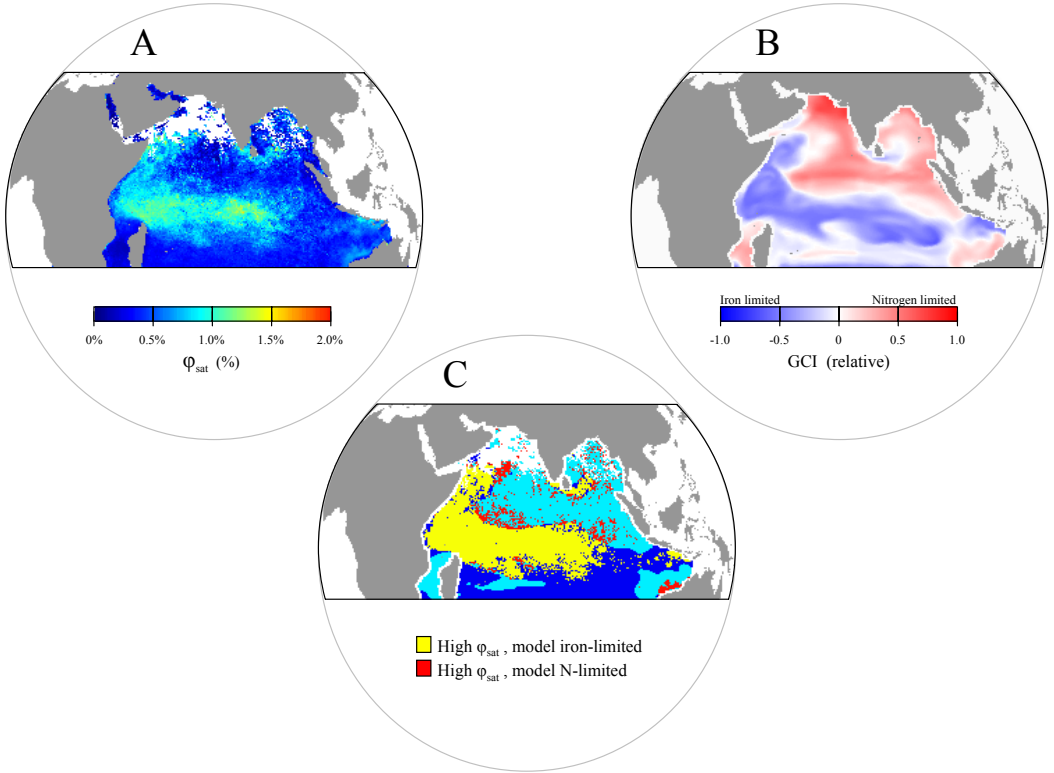

Fig. 6. Indian Ocean **(a)** ϕ_{sat} and **(b)** model-based GCI (Wiggert et al., 2006) for boreal summer (June–August). (b) Blue=Fe limited. Red = Nitrogen limited. **(c)** State-space comparison of ϕ_{sat} and GCI (colors as in Fig. 5c, f).

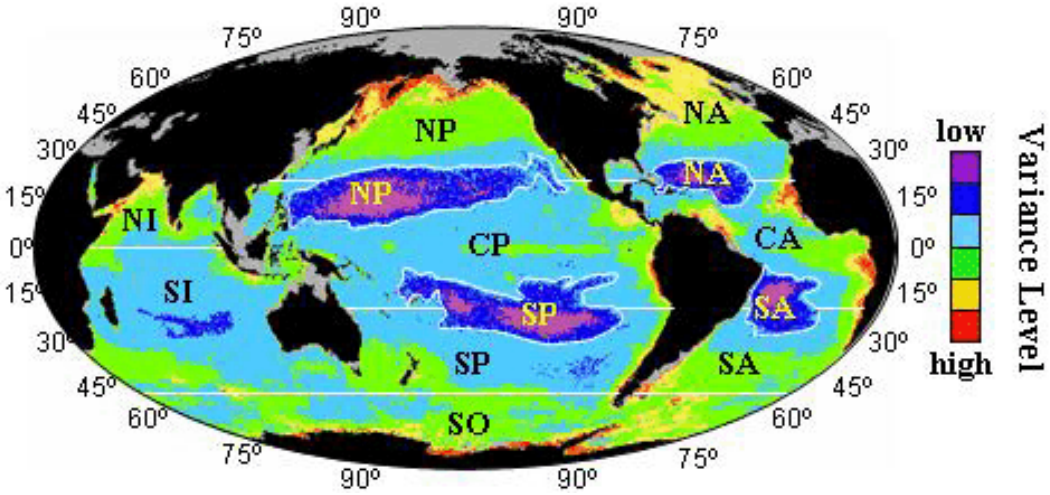

Fig. A1. For Fig. 2 of the manuscript, monthly F_{sat} data for the 5-year MODIS record were separated into 34 regional bins. Bin designations were based on annual variance in satellite chlorophyll concentration (Chl_{sat}) as described in Behrenfeld et al. (2005). The only difference between the current bin set and the earlier study of Behrenfeld et al. (2005) is that the Southern Ocean is now also divided into variance bins, rather than treating the entire region as a single bin. The 34 bins are distinguished here by ocean basin and color. NP, CP, SP = north, central, and south Pacific. NA, CA, SA = north, central, and south Atlantic. NI, SI = north and south Indian. SO = Southern Ocean. Colors indicate Chl_{sat} variability from lowest (purple) to highest (red). Gray indicates excluded areas.

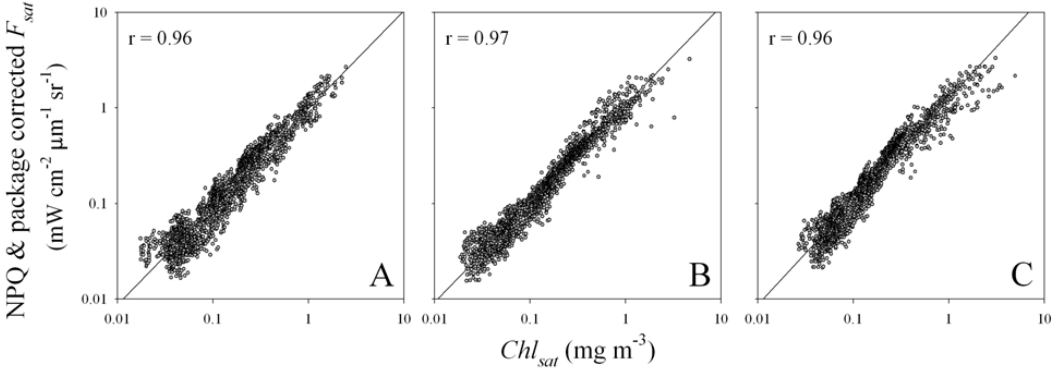

Fig. A2. Comparison of binned monthly F_{sat} data (corrected for NPQ and package effects) and satellite chlorophyll (Chl_{sat}) for three different chlorophyll algorithms. (a) MODIS standard empirical OC-3 algorithm. (b) Quasi-Analytical Algorithm (Lee et al., 2002). (c) Garver-Siegel-Maritorena semi-analytical algorithm (Maritorena et al., 2002). Correlation coefficients (r) for log-transformed data are shown in each panel. Panel (A) is identical to Fig. 2f in the main manuscript.